J Neuropathol Exp Neurol

Vol. 70, No. 6
June 2011
pp. 417–429

ORIGINAL ARTICLE

Impairment of Tight Junctions and Glucose Transport in Endothelial Cells of Human Cerebral Cavernous Malformations

Hannah Schneider, PhD, Mariella Errede, MD, PhD, Nils H. Ulrich, MD, Daniela Virgintino, MD, PhD, Karl Frei, PhD, and Helmut Bertalanffy, MD

Abstract

Cerebral cavernous malformations (CCMs) often cause hemorrhages that can result in severe clinical manifestations, including hemiparesis and seizures. The underlying mechanisms of the aggressive behavior of CCMs are undetermined to date, but alterations of vascular matrix components may be involved. We compared the localization of the tight junction proteins (TJPs) in 12 CCM specimens and the expression of glucose transporter 1 (GLUT-1), which is sensitive to alterations in TJP levels, in 5 CCM specimens with those in 5 control temporal lobectomy specimens without CCM by immunofluorescence microscopy. The TJPs occludin, claudin-5, and zonula occludens ZO-1 were downregulated at intercellular contact sites and partly redistributed within the surrounding tissue in the CCM samples; there was also a marked reduction of GLUT-1 immunoreactivity compared with that in control specimens. Corresponding analysis using quantitative real-time reverse transcription polymerase chain reaction on 8 CCM and 8 control specimens revealed significant downregulation of mRNA expression of occludin, claudin-5, ZO-1, and GLUT-1. The altered expression and localization of the TJPs at interendothelial contact sites accompanied by a reduction of GLUT-1 expression in dilated CCM microvessels likely affect vascular matrix stability and may contribute to hemorrhages of CCMs.

Key Words: Cerebral cavernous malformation, Claudin-5, GLUT-1, Occludin, Tight junctions, ZO-1.

INTRODUCTION

Cerebral cavernous malformations (CCMs) and arteriovenous malformations are the most common subtypes of brain vascular malformations, affecting more than 0.5% of the population (1–4). Cerebral cavernous malformations are composed of dilated blood-filled capillary clusters lined by endothelium and lacking intervening brain parenchyma. Based on their expression of angiogenic factors, they reflect more a developing rather than a mature vessel phenotype (1, 3, 5–7). Cavernous malformations occur sporadically as a single lesion or as an inherited autosomal dominant form with multiple lesions (8). To date, mutations in 3 genes associated with familial CCMs (i.e. *CCM1/KRIT1*, *CCM2/MGC4607*, and *CCM3/PDCD10*) have been identified (9). A second hit in the somatic allele may be necessary to cause CCM formation, and indeed, a biallelic *CCM1* somatic and germ line mutation was shown in a surgically excised human lesion for the first time (10); biallelic mutations have since been reported for *CCM2* and *CCM3* (11). Furthermore, transgenic mice heterozygous for *Ccm1* only develop CCM lesions when they exhibit an additional homozygous knockout of the tumor suppressor gene *Trp53* ($ccm1^{+/-}$ $Trp53^{-/-}$). Similarly, heterozygous mice ($Ccm2^{+/-}$) only form CCM lesions when sensitized by a second hit (12, 13), further supporting the hypothesis of a second genetic somatic mutation in CCMs.

Recently, it was shown that CCM1 represents an antiangiogenic protein, and that gene mutations in KRIT1 correlate with excessive capillary sprouting, which is also characteristic of human CCMs (7). Phosphatase and tensin homolog (PTEN) promoter methylation, heart of glass (HEG) transmembrane receptor expression, RhoA GTPase, and Rho kinase (ROCK) activation are involved in CCM pathogenesis and may contribute to mechanisms of their formation (14–17).

Endothelial cells (ECs) are the major component of vessel walls and likely play a central role in the clinical behavior of CCMs (18). The EC-lined thin walls of CCM channels possess a limited number of intact interendothelial tight junctions (TJs), which may contribute to their propensity for recurrent microhemorrhages (19). There is growing evidence that an impairment of the blood-brain barrier (BBB) correlates with a decrease of TJs in the endothelial layer, and furthermore, that CCM1 and CCM2 may play junction-stabilizing roles (15, 17, 20, 21). Recently, it was shown the EC TJ protein (TJP) occludin is involved in intercellular gap formation in porcine brain capillary ECs (22).

Tight junctions are located at the lateral apical side of the cell membrane in regions of close cell-to-cell contacts, such as in the cerebral microvascular endothelium. They turn cell-to-cell contacts into zones of tight adherence, thereby inhibiting the paracellular pathway for drugs or solutes from plasma into the central nervous system (23). Various integral membrane proteins, associated cytoplasmic proteins, and extracellular matrix components are involved in the proper assembly of TJ complexes (24). The junctional core proteins

From the Department of Neurosurgery, University Hospital, Zurich, Switzerland (HS, NHU, KF, HB); and Department of Human Anatomy and Histology, Bari University Medical School, Bari, Italy (ME, DV).
Send correspondence and reprint requests to: Hannah Schneider, PhD, University Hospital, Department of Neurosurgery, Frauenklinikstrasse 10, Zurich, 8091 Switzerland; E-mail: hannah.schneider@usz.ch
This research was supported by the Center for Clinical Research at the University of Zurich, Zurich, Switzerland.
Supplemental digital content is available for this article. Direct URL citations appear in the printed text and are provided in the HTML and PDF versions of this article on the journal's Web site (www.jneuropath.com).

occludin and claudin-5 play a key role in BBB integrity in the microvascular endothelium. Both consist of 4 transmembrane domains, intracellular N- and C-termini, and 2 extracellular domains that can interact with cell membranes of adjacent cells, thereby sealing the intercellular clefts (22, 25, 26). Different gain-of-function and loss-of-function experiments reveal that claudin-5 is involved in the structure of TJ strands and cell adhesion, whereas occludin probably has some accessory functions (27). The adaptor/scaffold proteins zonula occludens ZO-1, ZO-2, and ZO-3 connect TJ-associated integral membrane proteins to the actin cytoskeleton and other structural proteins. The first reported linker protein, ZO-1, directly interacts with occludin and claudins and is essential for TJ formation (27, 28). Because paracellular permeability increases when an imbalance occurs between occludin and ZO-1 molecules, the interaction of occludin with ZO-1 may modulate its function in sealing the junction (29, 30).

The localization of glucose transporter 1 (GLUT-1) in ECs of microvessels is considered to indicate a functioning BBB (31–33). The GLUT-1 is widely expressed in adult tissues, but it is most abundant in fibroblasts, erythrocytes, and ECs with low levels of expression in muscle, liver, and adipose tissue (34–36). In healthy brain endothelium, TJ sealing of the interendothelial clefts is linked to the expression of GLUT-1. Alterations in transporter protein expression are directly related to an increased permeability of EC layers in the brain and linked to alterations in TJ properties (31–33).

The role of TJs and their core proteins occludin and claudin-5 is not understood in the context of CCMs, but there is growing evidence that vascular development and endothelial permeability are dysregulated in them (37). Decreased expression of GLUT-1 is coupled to alterations in TJP expression levels and consequent BBB permeability in glioblastomas (38). Therefore, we analyzed the expression of the TJPs occludin, claudin-5, and ZO-1, and the transporter protein GLUT-1 by immunohistochemistry and confocal fluorescent microscopy on cryosections and paraffin sections of 7 CCM specimens and 5 control tissue samples from patients with temporal lobe epilepsy. Mean fluorescence intensities (FIs) were further quantified. Quantitative reverse transcription polymerase chain reaction (RT-PCR) was also performed to compare mRNA expression levels of TJPs and GLUT-1 in 8 CCM specimens and 8 control samples.

MATERIALS AND METHODS

Patients and Tissue Specimens

The CCM specimens (n = 12) were obtained from patients undergoing neurosurgical resection. The patients studied fulfill the consensus recommendations for minimal reporting variables in CCM clinical research (39–41). The decision for surgical resection was made based on computed tomographic scans and magnetic resonance images. The clinical data of the 12 CCM patients are summarized in Table 1. Control specimens (n = 13) were from temporal lobes obtained during selective amygdalohippocampectomy in 12 patients with temporal lobe epilepsy. The median age of the 7 female patients and the 6 male patients was 38 years (range, 23–52 years). Tissue specimens were immediately transferred to the laboratory on ice and divided for snap-frozen preparation and in-vitro experiments. Samples were snap frozen in liquid nitrogen and embedded in TissueTek OCT (Sakura Finetek Europe, Zoeterwoude, Netherlands) before analysis. In addition, histological diagnosis was obtained by routine clinical neuropathologic examination and classified according to the World Health Organization criteria at the Institute of Neuropathology, University Hospital, Zurich, Switzerland.

Immunofluorescence, Laser Scanning Confocal Microscopy, and Fluorescence Microscopy Analysis

Immunofluorescence analysis was done using 3 different protocols. First, 6-μm-thick cryosections were cut with a

TABLE 1. CCM Patient Data

	Clinical Parameters				CCM Characteristics			
Patient No.	Age, Years/Sex	Clinical Presentation	Radiological Findings	Family History	Lesion Location	Size (Diameter), mm	Multiple Lesions	DVA
CCM1	38/M	SH	RH	N	R parietal			N
CCM2	23/F	SH	RH	N	R brachium pontis			N
CCM3	48/F	SH	NRH	Y	L brachium pontis			N
CCM4	34/F	NH-FND	NRH	N	L cerebral peduncle	29	N	Y
CCM5	36/F	SH	RH	N	L insula	10	Y	Y
CCM6	6/M	SH	NRH	N	R pons	12	Y	N
CCM7	14/F	SH	NRH	N	R pons	14	N	N
CCM8	35/F	NH-FND	NRH	N	L pons	9	N	Y
CCM9	7/F	NH-FND	NRH	N	R subinsula	23	N	N
CCM10	27/F	SH	RH	N	L pons	20	N	Y
CCM11	39/M	NH-FND	RH	N	R occipital	15	N	N
CCM12	47/F	SH	NRH	N	Pons	20	N	Y

All patients were white.

CCM, cerebral cavernous malformation; DVA, developmental venous anomaly associated with the CCM; F, female; L, left; M, male; N, no; NH-FND, nonhemorrhagic focal neurological deficit; NRH, no recent hemorrhage; R, right; RH, recent hemorrhage; SH, symptomatic hemorrhage; Y, yes.

TABLE 2. Primer Sequences for qRT-PCR

Occludin forward	CACACAGGACGTGCCTTCAC
Occludin reverse	GAGTATGCCATGGGACTGTCAA
Claudin-5 forward	CTGCTGGTTCGCCAACATT
Claudin-5 reverse	TGCGACACGGGCACAG
ZO-1 forward	CAGCCGGTCACGATCTCCT
ZO-1 reverse	TCCGGAGACTGCCATTGC
GLUT-1 forward	TGCTCATGGGCTTCTCGAA
GLUT-1 reverse	AAGCGGCCCAGGATCAG
CD31 forward	TCTCCCAGCCCAGGATTTC
CD31 reverse	TTCGATGGTCTGTCCTTTTATGAC
vWF forward	AGAAACGCTCCTTCTCGATTATTG
vWF reverse	TGTCAAAAAATTCCCCAAGATACA

GLUT-1, glucose transporter 1; qRT-PCR, quantitative real-time reverse transcription polymerase chain reaction; vWF, von Willebrand factor; ZO-1, zonula occludens 1.

Leica cryostat, mounted on Superfrost Plus slides (Menzel-Glaser, Braunschweig, Germany), fixed with acetone p.a. for 10 minutes at room temperature (RT), and stored at −80°C until further use. For analysis, slides were acetone fixed for 5 minutes at RT and air-dried. Sections were incubated with 3% hydrogen peroxide to quench endogenous peroxidase activity and washed with PBS (pH 7.4). Unspecific binding sites were blocked with blocking solution (Candor, Weißensberg, Germany) for 25 minutes at RT. For indirect immunofluorescence, polyclonal rabbit anti-human claudin-5 antibody (5 μg/mL; Abcam, Cambridge, UK), monoclonal mouse anti-human occludin antibody (4 μg/mL; Invitrogen, Carlsbad, CA), monoclonal mouse anti-human GLUT-1 antibody (1 μg/mL; Abcam), monoclonal mouse anti-human fibronectin (2 μg/mL; Abcam), mouse monoclonal anti-human CD31 (10 μg/mL; DAKO, Glostrup, Denmark), monoclonal rabbit anti–human CD31 (1:40; Epitomics, Burlingame, CA), monoclonal mouse anti-human collagen IV antibody (2 μg/mL; DAKO), and polyclonal rabbit anti-human collagen VI antibody (2 μg/mL; Abcam) were incubated at 37°C for 1 hour. Appropriate secondary antibodies, Alexa Fluor 488–conjugated (goat anti-rabbit and goat anti-mouse, 1:100) or Alexa Fluor 594–conjugated secondary antibody (goat anti-rabbit and goat anti-mouse, 1:100) (all from Invitrogen) were incubated for 25 minutes at RT. All antibodies were diluted in antibody dilution buffer (DCS, Hamburg, Germany). Between each step, the sections were washed in PBS 3 times for 5 minutes each. Staining controls included the isotype-matched primary monoclonal antibodies. In all cases, the result of each negative control confirmed the specificity of the corresponding antibody staining. Specimens were mounted in fluorescent mounting medium (DAKO) and were viewed on a Leica TCS SP5 (Leica, Wetzlar, Germany) confocal laser scanning microscope using 63× and 100× objectives. Confocal images were taken at 1- to 2-μm intervals through the z axis of the section. Projection images formed by serial optical planes were analyzed, digitally recorded, and stored as tagged image file format (TIFF) files using Adobe Photoshop CS3 software (Adobe Systems, San Jose, CA). Second, tissue samples were placed in 4% neutral buffered formalin for 12 hours and then processed routinely for paraffin embedment. Sections were obtained at 4-μm intervals using a Microm rotary microtome (Leica) and mounted on Superfrost Plus slides (Menzel-Glaser). After rehydration, the sections were boiled in a microwave oven in 0.01 mol/L citrate buffer solution (pH 6) for 20 minutes for antigen retrieval. Endogenous peroxidase was inactivated with 3% hydrogen peroxide, and nonspecific antigenic sites were blocked with blocking solution (Candor) for 25 minutes at RT. As previously described, the sections were incubated with primary occludin antibody (4 μg/mL; Invitrogen), GLUT-1 antibody (1 μg/mL; Abcam), and polyclonal rabbit anti–human von Willebrand factor (vWF) antibodies (28.5 μg/mL; DAKO) followed by incubation with appropriate secondary antibodies, Alexa Fluor 488–conjugated secondary antibody (goat anti-mouse, 1:100; Invitrogen) or Alexa Fluor 594–conjugated secondary antibody (goat anti-rabbit, 1:100; Invitrogen). Third, the specimens were fixed for 3 hours at 4°C by immersion in 2% paraformaldehyde plus 0.2% glutaraldehyde solution and washed in PBS (pH 7.6). The blocks of tissue were sectioned at 20-μm thickness using a vibrating microtome (Leica), and the sections were collected on polylysine slides (Menzel-Glaser). Heat-mediated antigen retrieval was achieved by microwave pretreatment in 0.01 mol/L citrate buffer (pH 6.0) for 15 minutes at 750W. Sections were incubated with PBS/0.5% Triton X-100 for 30 minutes, blocked with serum-free protein block (DAKO) for 15 minutes at RT, and incubated overnight at 4°C with primary antibodies at various dilutions: mouse monoclonal anti–human claudin-5 (1:20; Zymed Laboratories, Invitrogen), rabbit polyclonal anti–human occludin (1:50; Zymed), rabbit polyclonal anti–human collagen IV (1:200; Acris Antibodies, Hiddenhausen, Germany), mouse monoclonal anti–human collagen IV (1:50; DAKO), and mouse monoclonal anti–human CD31 (1:50; DAKO). A mixture of biotinylated horse anti-mouse IgG (1:400; Vector Laboratories, Inc, Burlingame, CA) or biotinylated goat anti–rabbit IgG (1:400; Vector Laboratories) and Alexa Fluor 568–conjugated goat anti–rabbit IgG (1:400; Invitrogen) or Alexa Fluor 555–conjugated goat anti-mouse IgG (1:400, Invitrogen) were incubated as secondary antibodies for 40 minutes at RT. Streptavidin Alexa Fluor 488–conjugated antibody (1:400; Invitrogen) was used for staining of claudin-5 and occludin. The slices were counterstained with TO-PRO-3 (1:10000 in PBS; Invitrogen) and finally mounted with Vectashield (Vector Laboratories) and sealed with nail varnish. The slices were examined under the Leica TCS SP5 confocal laser scanning microscope using a sequential scan procedure during image acquisition of double label sections. Confocal images were taken at 250- to 500-nm intervals through the z axis of the sections. Images from individual optical planes and image projections of stacks of serial optical planes were analyzed by confocal software (Multicolor Package, Leica).

Image Acquisition, Image Processing, and Data Analysis

Digital image processing for the detection and quantification of FI in human CCM and control samples was performed with a conventional light microscope (Axiovert 100, Zeiss, Jena, Germany), a digital microscope camera (AxioCam ICm, Zeiss), and the AxioVision 4.8 software (Zeiss). Fluorescence quantification was subdivided into image acquisition,

image preprocessing, and data processing steps (42). All parameters used in the acquisition (i.e. detector gain and exposure time) were standardized to maximize reproducibility. Image processing of each specimen was provided through region of interest (ROI) analysis. The software allows the interactive definition of areas for size and intensity measurements. For data analysis, FI/ROI values were obtained for 5 ROI per specimen (10 μm^2 each). Statistical analysis describing the distribution of FI signals was performed to obtain graphic representations.

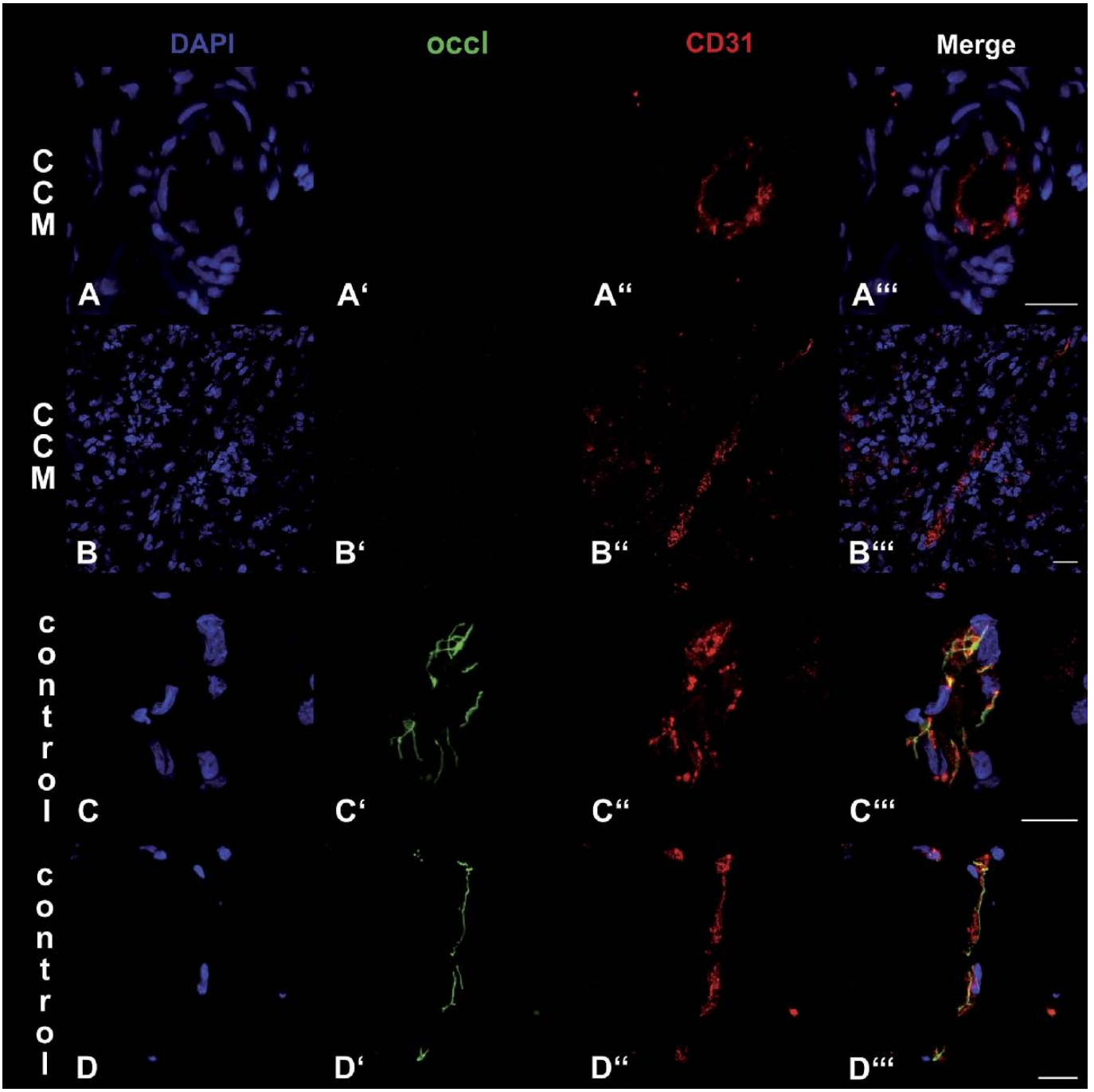

FIGURE 1. Localization of the tight junction protein occludin (green) in cerebral cavernous malformations (CCMs). Confocal z series projections of CCM1, CCM2 **(A, B)**, and control samples C2 and C4 **(C, D)**. Occludin is distributed in a linear pattern along vessels of control tissues **([C′]** cross sectional; **[D′]** longitudinal). Occludin is redistributed and shows decreased expression in endothelial cells (ECs) of CCMs **([A′]** cross sectional; **[B′]** longitudinal). The EC marker protein PECAM-1 (CD31) is stained red **(A″–D″)**. The 4′,6-diamidino-2-phenylindole (DAPI) staining (blue) is shown in **(A)** to **(D)** and merged images in **(A‴)** to **(D‴)**. Scale bars = 20 μm.

Quantitative RT-PCR Analysis

Differential gene expression levels of claudin-5, occludin, ZO-1, and GLUT-1 were determined by quantitative RT-PCR. Total RNA was isolated from each CCM and control tissue sample using the RNeasy Mini Kit Isolation System according to the manufacturer's protocol (Qiagen Ltd, Hombrechtikon, Switzerland); 0.5 μg total mRNA of each sample was reverse transcribed to cDNA using the High Capacity cDNA Reverse Transcription Kit (ABI, Carlsbad, CA). Complementary DNA was used for quantitative RT-PCR with

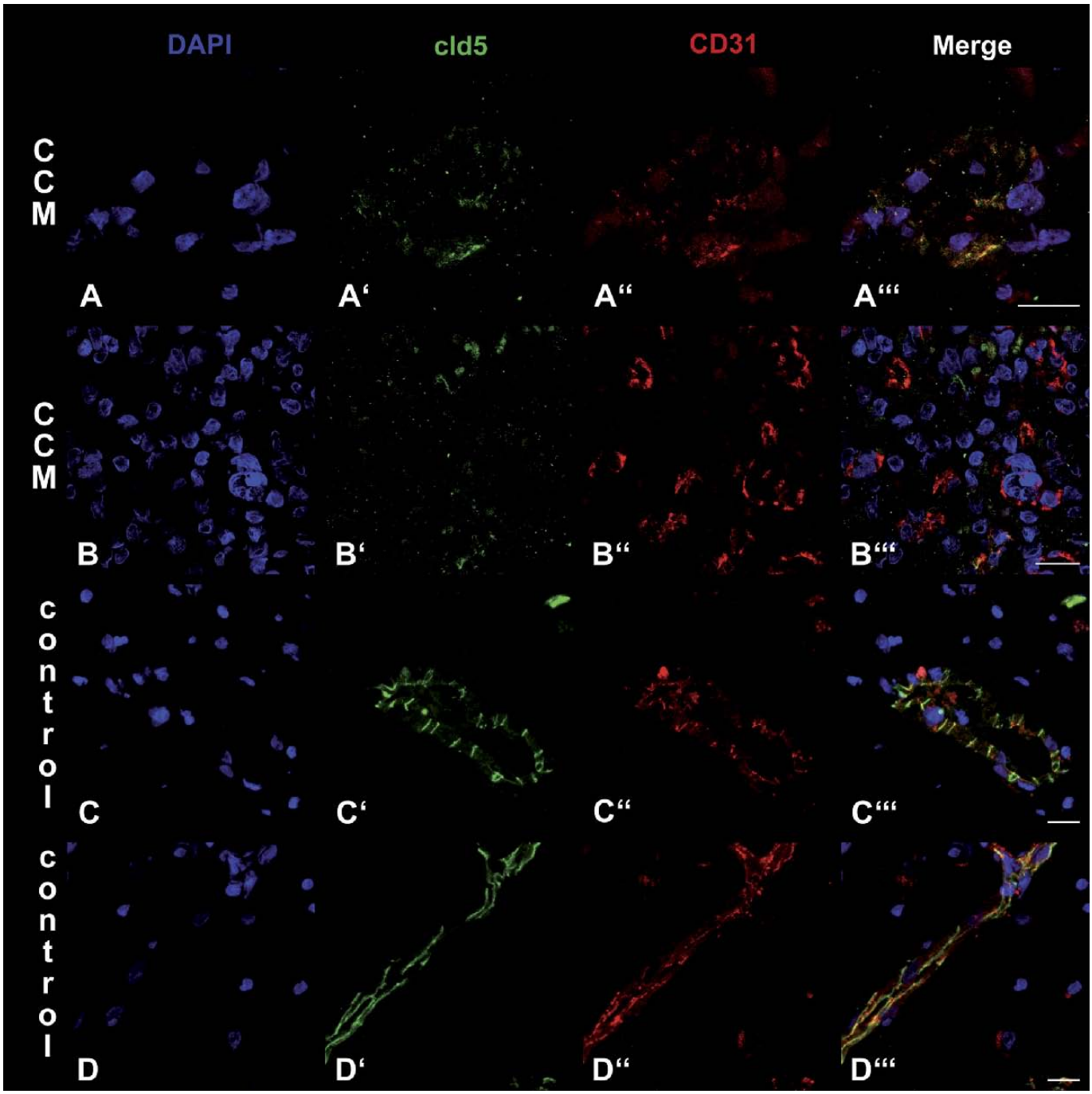

FIGURE 2. Distribution of claudin-5 (cld-5, green) and localization of the endothelial cell (EC) marker CD31 in cerebral cavernous malformations (CCMs) by confocal microscopy. **(A–D)** The CCM specimens CCM2 and CCM3 **(A, B)** and controls c2 and c4 **(C, D)** are shown. Claudin-5 (as for occludin) is distributed linearly in vessels of control tissues (**[C′]** cross sectional; **[D′]** longitudinal). Claudin-5 expression is decreased in CCM ECs (**[A′, B′]** cross sectional). The PECAM-1 (CD31) is stained red **(A″–D″)**; 4′,6-diamidino-2-phenylindole (DAPI) staining (blue) is shown in **(A)** to **(D)**; merged images are in **(A‴)** to **(D‴)**. Scale bars = 20 μm.

SYBR Green PCR Master Mix (ABI) and specific primer pairs on a 7900HT Fast Real-Time PCR System with SDS Software v2.4 (ABI). Expression was normalized against the endothelial marker CD31 or vWF. Specific primers were designed with the Primer Express 3.0 software (ABI) (Table 2).

Statistical Analysis

For quantification and statistical analysis of protein expression levels, experiments were done in triplicate, analyzing 5 ROI per specimen (10 μm^2) for each patient. Mean FI values were calculated and averaged. Regions of interest were

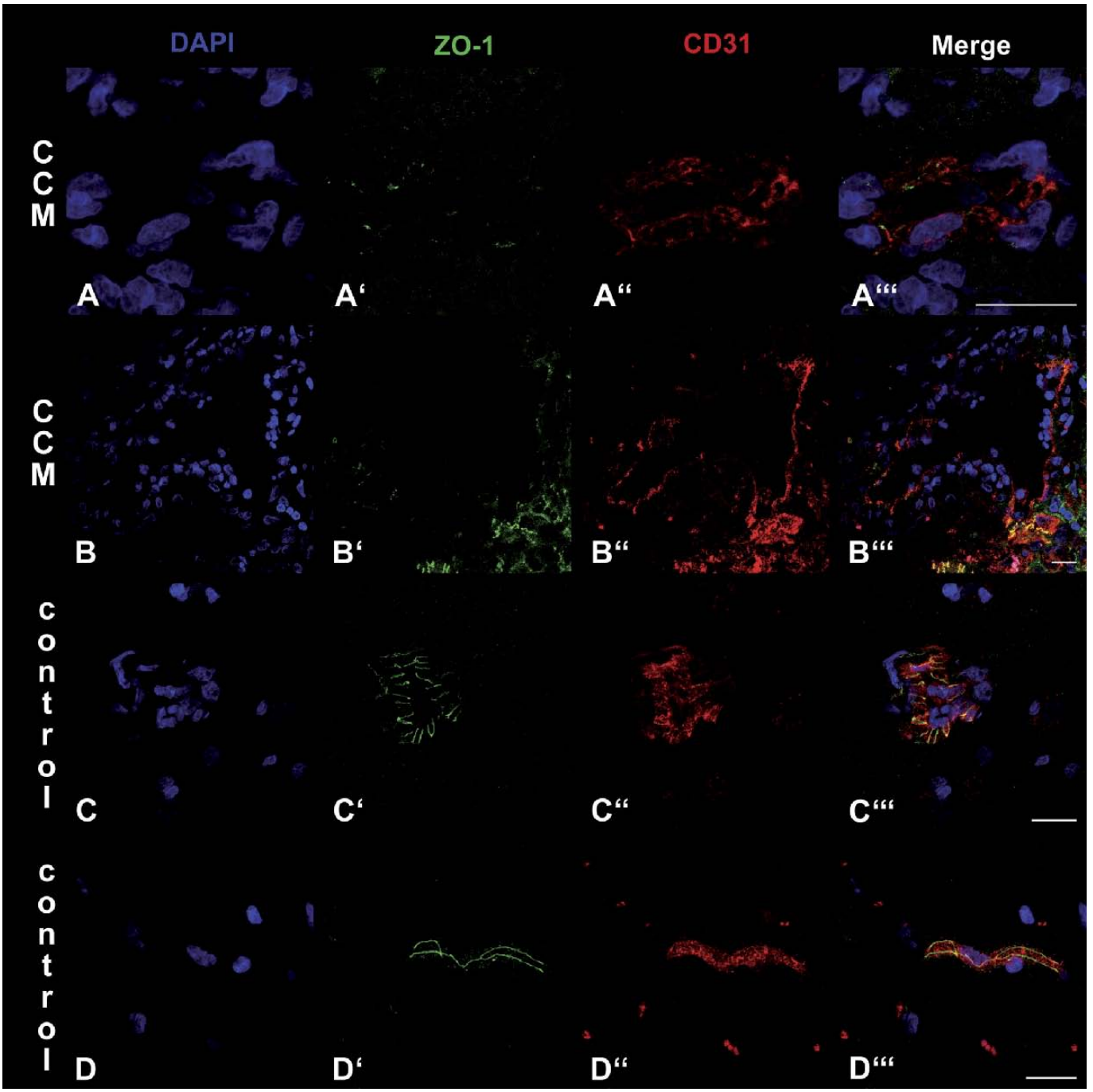

FIGURE 3. Confocal microscopic images of zonula occludens ZO-1 (green) and CD31 (red) in cerebral cavernous malformation (CCM) (CCM2, CCM3) and control specimens (c1, c4). **(A–D)** The ZO-1 staining in controls is distributed in a typical linear vessel pattern (**[C′]** cross sectional; **[D′]** longitudinal). In contrast, ZO-1 is markedly decreased (**[A′, B′]** cross sectional) in CCM samples. The 4′,6-diamidino-2-phenylindole (DAPI) staining (blue) is mapped in **(A)** to **(D)**; merged images are in **(A‴)** to **(D‴)**. Scale bars = 20 μm.

randomly selected by criteria that only fluorescent signals of vessel wall structures were measured for their intensity. The statistical analysis, using the mean FI values of each patient, was performed with Microsoft Excel and GraphPad Prism software (version 5 for Windows). An unpaired Student *t*-test was used to assess whether 2 independent samples

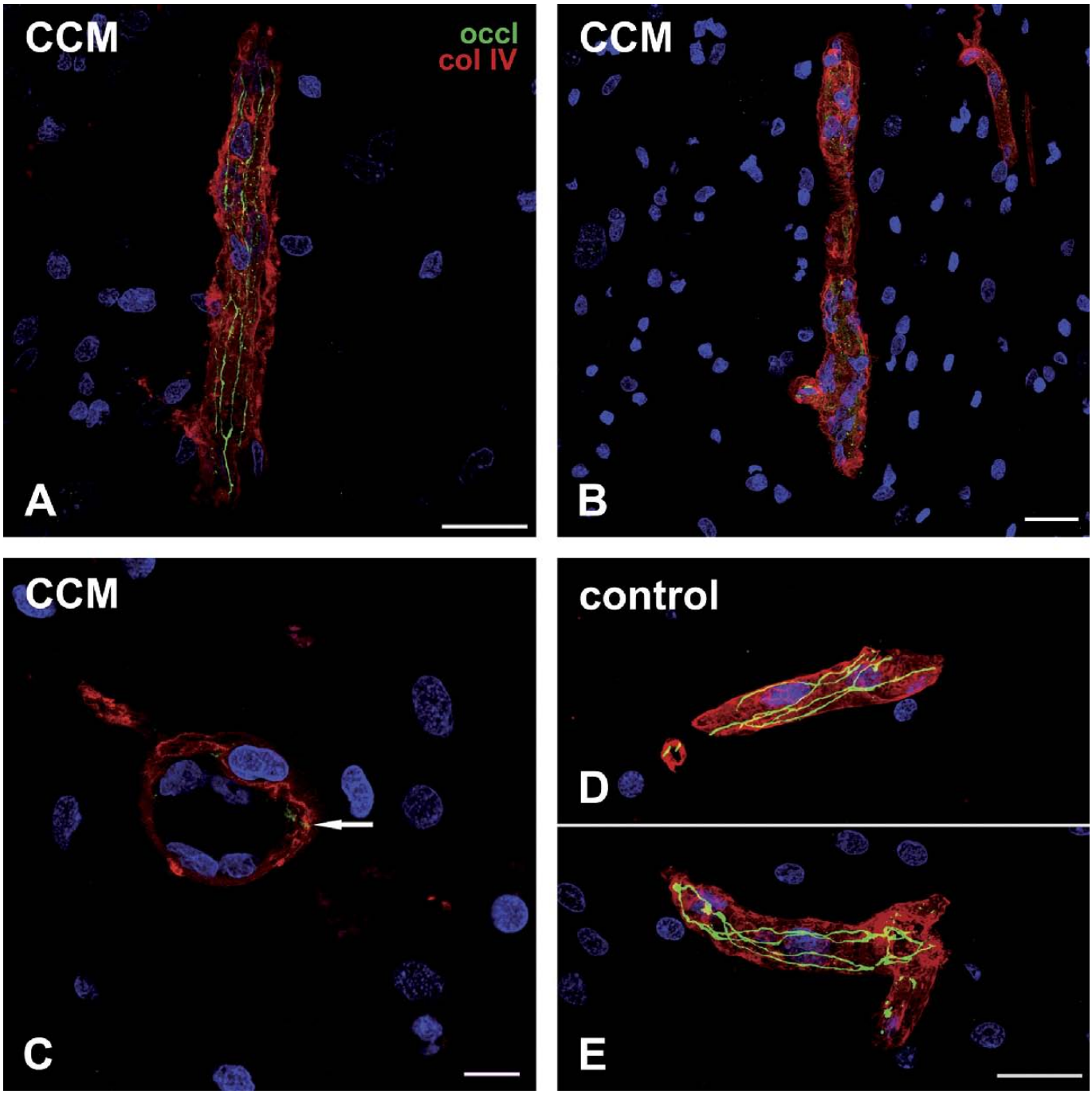

FIGURE 4. Immunostaining for occludin (occl, green) and collagen IV (col IV, red) in 2 cerebral cavernous malformation (CCM) and control brain tissue samples, respectively. **(A–C)** There are different patterns of occludin distribution. As in control vessels, the linear pattern of occludin staining in CCM is preserved but thinned (**[A]** longitudinal). To some extent, occludin is arranged in a punctate pattern along cell-to-cell contacts (**[B]** longitudinal). At other foci, vessels are completely unstained along the major length of their profile but show isolated residual protein aggregates (arrow) (**[C]** cross sectional). **(D, E)** Occludin is distributed in a linear pattern in microvessels in the control brain (cerebral cortex). Basement membranes of capillaries are labeled with anti–collagen IV antibody, and nuclei are stained with TO-PRO3 (blue), as shown in **(A)** to **(E)**. Scale bars = **(A, B, D, E)** 25 μm; **(C)** 10 μm.

of observations came from the same distribution. Values of $p < 0.01$ were considered significant.

Messenger RNA expression levels of each gene were obtained via correction for endothelial density. The results are expressed as mean ± SEM. Statistical evaluation was performed with the GraphPad Prism software. Statistical significance was determined by Mann-Whitney-Wilcoxon test. Values of $p < 0.05$ were considered statistically significant.

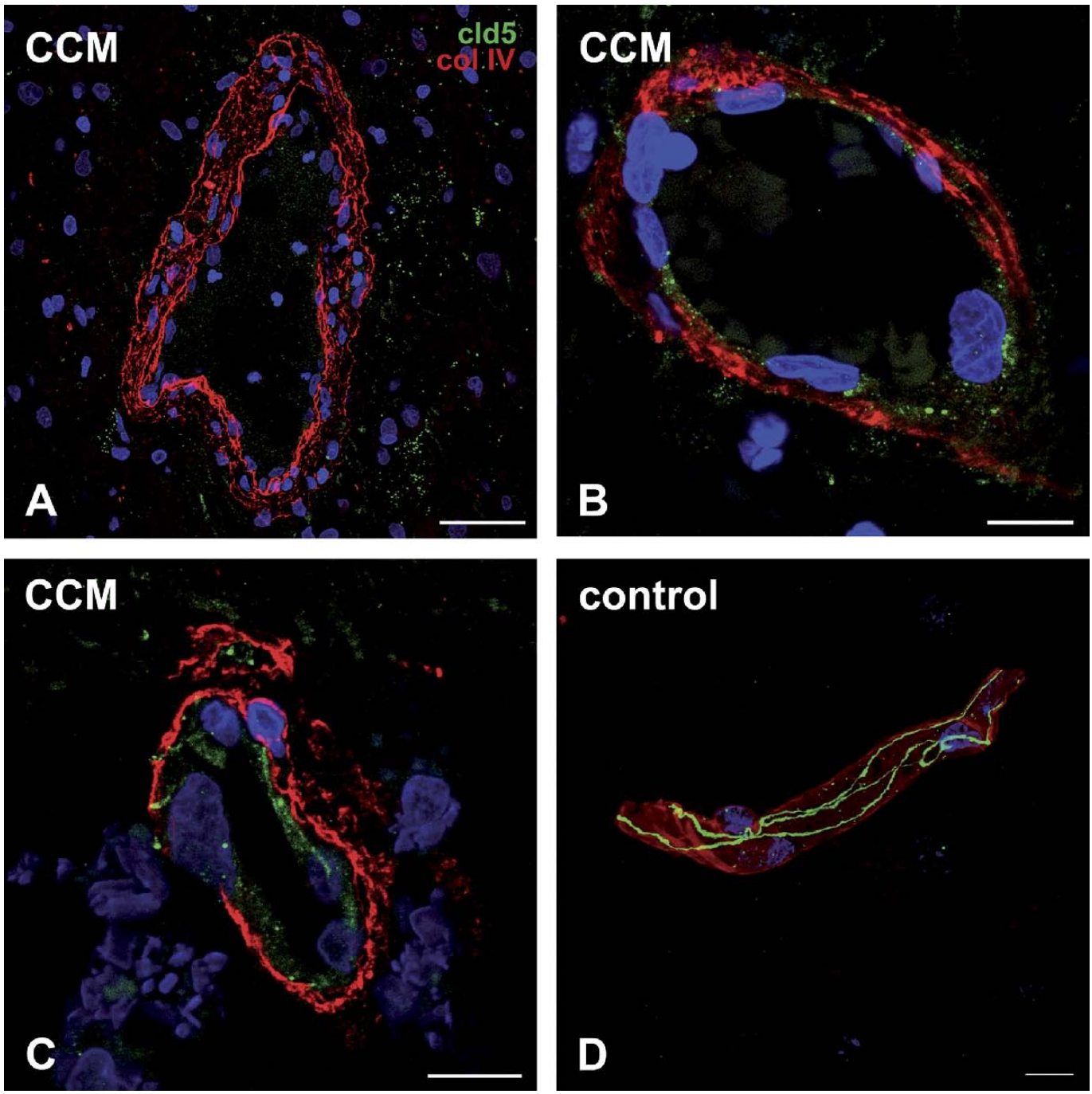

FIGURE 5. Immunostaining for claudin-5 (cld-5, green) and collagen IV (col IV, red) in 2 cerebral cavernous malformation (CCM) and control specimens. **(A–D)** In most instances, vessels seem negative for claudin-5; in some foci, claudin-5 is diffusely distributed within the tissue and not localized to intercellular contact sites (**[A]** cross sectional). A few vessels show a punctate staining pattern (**[B]** cross sectional). Decreased claudin-5 staining is seen along the EC contacts (**[C]** cross sectional). Linear claudin-5 staining in capillaries of a control sample (**[D]** longitudinal). Microvessel basement membranes are labeled for collagen IV; nuclear staining with TO-PRO3 (blue) is shown in **(A)** to **(C)**. Scale bars = **(A, D)** 30 μm; **(B, C)** 10 μm.

RESULTS

TJP Expression in CCM and Control Microvessels

Sections stained for the EC marker protein platelet/endothelial cell adhesion molecule 1 (PECAM-1)/CD31 on cryosections (Figs. 1–3A″–D″) and vWF on paraffin sections (Figure, Supplemental Digital Content 1, http://links.lww.com/NEN/A239) showed a typical linear staining pattern at distinct EC borders in control samples. Occludin, claudin-5, and ZO-1 immunoreactivities were clearly decreased in endothelial layers of CCM tissue

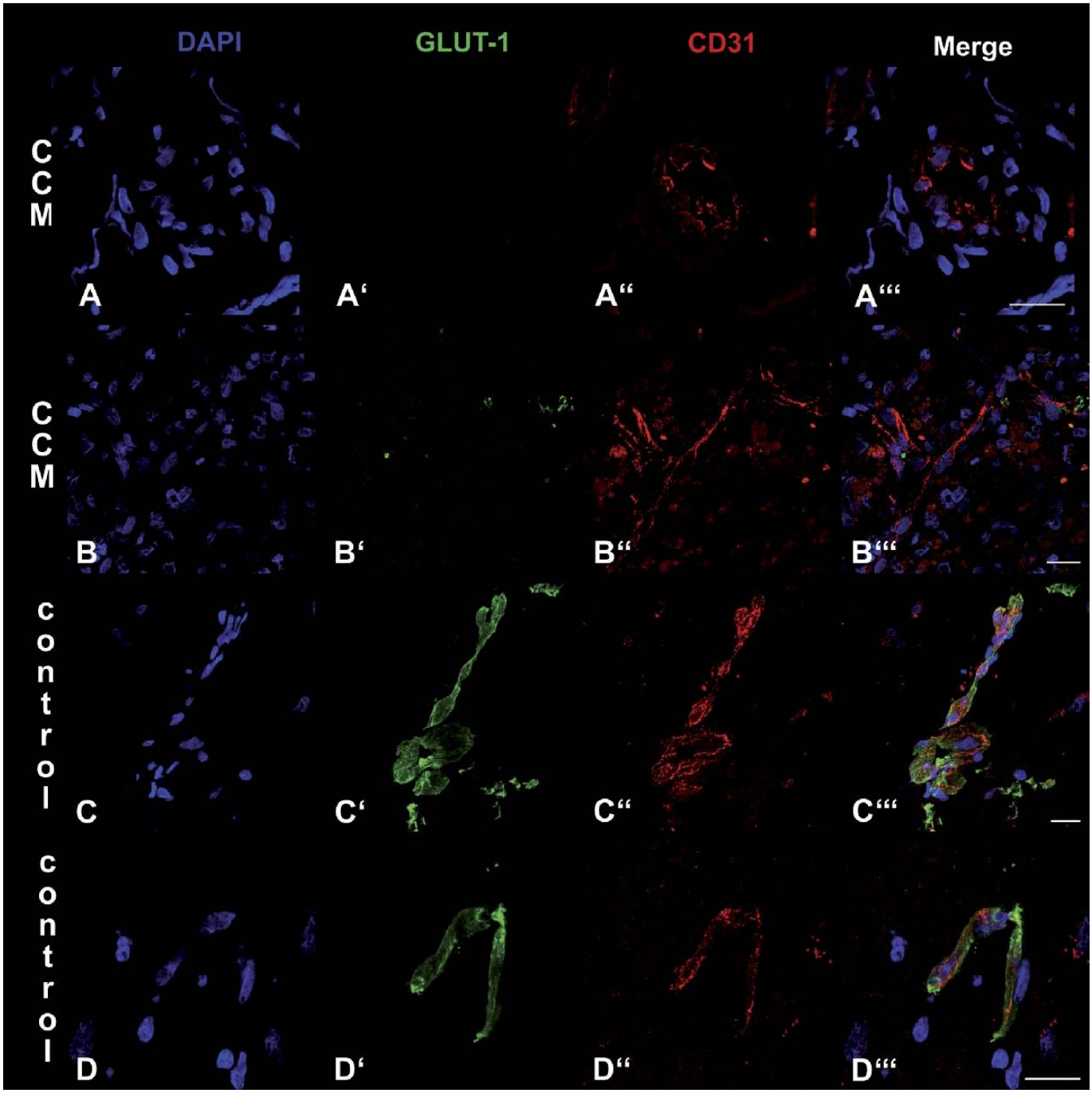

FIGURE 6. Confocal imaging of cryosections of cerebral cavernous malformation (CCM) (CCM1, CCM6) and control brain tissues (c1, c5) immunostained for glucose transporter 1 (GLUT-1) (green) and CD31 (red). (A–D) In control vessels, GLUT-1 is distributed uniformly (**[C′]** cross sectional/longitudinal; **[D′]** longitudinal). The GLUT-1 staining is markedly reduced in CCM tissue samples (**[A′]** cross sectional; **[B′]** cross sectional/longitudinal). Non-EC staining in **(C′)** and **(C‴)** likely represents extravasated erythrocytes. The 4′,6-diamidino-2-phenylindole (DAPI) staining (blue) is mapped in **(A)** to **(D)** and merged images in **(A‴)** to **(D‴)**. Scale bars = 20 μm.

compared with control brain microvessels (Figs. 1–4; Figure, Supplemental Digital Content 1, http://links.lww.com/NEN/A239). The linear junctional labeling was either discontinuous or amorphous, and many vessels even seemed negative for TJPs. In several cases, redistribution of proteins was observed in the endothelial layer, as well as the surrounding tissue (Figs. 1–3A′–C′). Costaining for CD31 and vWF additionally revealed that only microvessels were analyzed for TJP localization.

We next built 3-dimensional reconstructions of vascular structures to validate the immunofluorescence experiments that showed different localization patterns for TJPs along the margin of cell-to-cell contacts and in the surrounding tissue of CCMs when compared with controls (Figs. 4, 5). In regions of CCM tissue where a protein signal could be determined, few vessels showed a punctate labeling for claudin-5 (Figs. 4B, C; 5A, B); in others, occludin and claudin-5 were linearly arranged along the cell-to-cell contacts (Figs. 4A, 5C). In those cases, the fluorescence signal of both proteins was clearly less than that in the control samples. Furthermore, in the control tissues, occludin and claudin-5 staining was limited to the vascular intima (Figs. 4D, E; 5D) and was also detected in the surrounding tissue in some regions of the CCM sections (Fig. 5A).

GLUT-1 Expression in CCM Vessels

Because BBB permeability not only corresponds to alterations in TJPs, but to an impairment of GLUT-1 expression, CCM and control tissue cryosections were immunostained for this transmembrane transporter protein in cryosections (Fig. 6) and paraffin sections (Supplemental Digital Content 2, http://links.lww.com/NEN/A241). Microvessels of control brain samples uniformly showed a high level of GLUT-1 staining, whereas GLUT-1 expression was markedly reduced or absent in CCM specimens (Fig. 6; Figure, Supplemental Digital Content 2, parts A-B, http://links.lww.com/NEN/A241). As an internal positive control, GLUT-1 immunoreactivity on erythrocytes was observed in every sample (Fig. 6C′). Irregular fibronectin staining around CCM microvessels indicated BBB impairment (Fig. 7).

Protein Expression Levels

There was a marked reduction of TJP and GLUT-1 levels along EC borders that corresponded to decreased FI per ROI (Fig. 8). Lower occludin, claudin-5, ZO-1, and GLUT-1 fluorescence signals were demonstrated in each CCM specimen (Fig. 8A). Slight differences in the extent of protein reduction were likely caused by different tissue compositions of each CCM sample. Mean values calculated for CCMs and controls revealed an FI signal reduction of 62% for occludin, 71% for claudin-5, and 74% for ZO-1 in CCM tissue versus those in control tissue (Fig. 8B). The decrease of FI per protein expression in CCM vessels was highly significant in all cases ($p < 0.0001$). The most striking decrease of protein expression in CCM vessels versus controls was found for GLUT-1 (78%) ($p < 0.0001$).

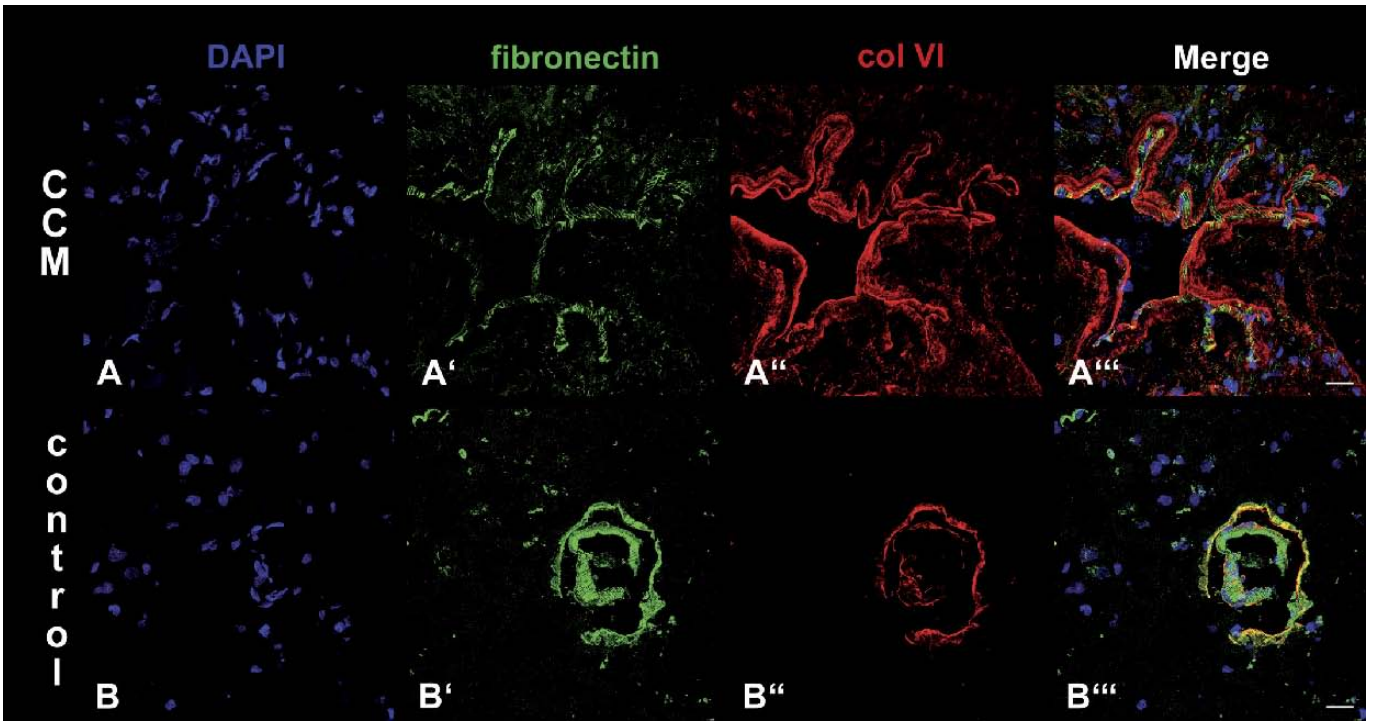

FIGURE 7. Localization of fibronectin (green) and collagen VI as an endothelial cell (EC) marker (**[A″, B″]** red) in cerebral cavernous malformation (CCM) (CCM5) and control (c1) samples by confocal microscopy **(A, B)**. Fibronectin is uniformly distributed in vessels of the control sample (**[B′]** cross sectional). In CCM EC, there is less fibronectin expression, and the pattern is irregular (**[A′]** cross sectional). The 4′,6-diamidino-2-phenylindole (DAPI) staining (blue) is shown in **(A)** and **(B)** and merged images in **(A‴)** and **(B‴)**. Scale bars = 20 μm.

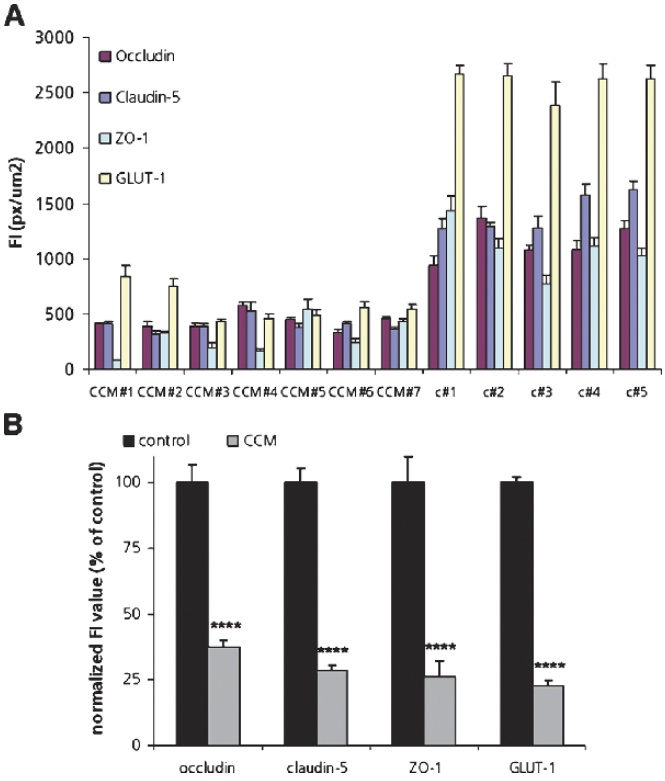

FIGURE 8. Analysis of fluorescent intensity (FI) of occludin, claudin-5, zonula occludens ZO-1, and glucose transporter 1 (GLUT-1) staining in cryosections of cerebral cavernous malformation (CCM) and control tissues. Experiments were done in triplicate. **(A)** Mean FI of each CCM and control specimen. **(B)** Mean FI (in percentage) of the 7 normalized CCM specimens versus controls. Mean control FI was calculated as 100% (mean ± SEM). Changes in mean FI were highly significant for all proteins examined (Student *t*-test, **** $p < 0.0001$).

Messenger RNA Expression

To validate the immunohistochemistry findings, we performed real-time RT-PCR and normalized against either endothelial marker CD31 (Fig. 9) or vWF (not shown); these analyses showed similar results. Total RNA expression from 8 samples was analyzed for each group of CCM and controls. The RNA expressions of occludin (13% ± 3.6%), claudin-5 (25.8% ± 8.3%), and ZO-1 (8.2% ± 3.6%) were significantly decreased in CCM versus control samples (Mann-Whitney-Wilcoxon test, $p < 0.05$). The GLUT-1 expression was also significantly reduced (15.8% ± 4.3%) when compared with RNA expression in control samples.

DISCUSSION

We report that the expressions of TJPs and of GLUT-1 are decreased in CCMs compared with those in control samples. The expression of TJPs was markedly reduced at interendothelial contact sites and seemed negative in most of the vessels. The structural composition of TJs in ECs of brain capillaries is highly complex (43), and impairment of TJ assembly may lead to a loss of BBB integrity (44–48). Occludin and claudin-5 are critical for proper BBB function and permeability, and immunoreactivity for these proteins was decreased at interendothelial contact sites in CCM tissue. Furthermore, the expression of the TJ-associated protein ZO-1 was also altered. The ZO-1 and occludin are considered to be the most important protein components for the maintenance of the BBB (49–52); claudin-5 plays an essential role in TJ formation, generating the structural and functional core of the multiprotein complex (27). The resulting incorrect assembly of TJs may lead to a malfunctioning BBB. Moreover, downregulation of ZO-1 suggests a disturbance in interaction of TJs with the actin cytoskeleton, likely affecting the physiology of the CCMs. The ZO-1 loss might lead to the disruption of the cellular architecture and a mismatch between interacting TJPs that result in cellular instability. Indeed, overexpression of occludin and inadequate levels of ZO-1 impair BBB function (29). In addition, occludin phosphorylation correlates with TJ formation, regulation of junction permeability, and interaction with ZO-1 (53–55). Claudin-5 is a key determinant of transendothelial resistance at the BBB, and alterations in its interacting proteins can also lead to a disruption of the barrier function (53). The deviations of TJP protein localization were accompanied by protein redistribution within the surrounding brain parenchyma of CCM vessels. Taken together, our observations suggest that cell-to-cell contacts of CCM vessels are disorganized, and that TJ proteins are redistributed in parts of the EC surrounding tissue. Quantification of signal intensities of TJP expression confirmed our immunohistochemical observations.

Alterations of TJ assembly in CCMs leading to a malfunctioning permeability barrier are also reported in brain tumor vessels and in brain capillaries after ischemic events (22, 38, 56). In many patients, CCM pathology comprises repeated microhemorrhages into the surrounding brain parenchyma, corresponding to an impaired permeability of the vascular channels. On the other hand, CCM vessels are not devoid of correctly assembled TJ complexes; although expression was

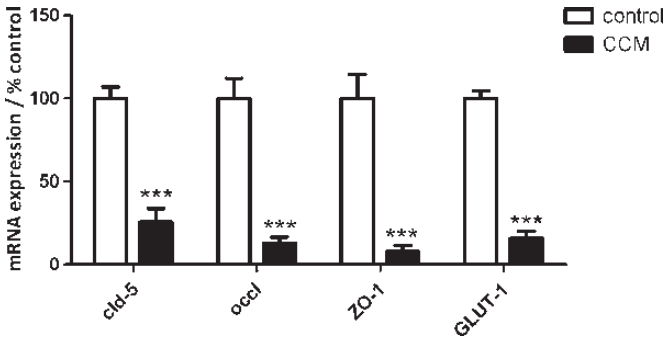

FIGURE 9. Relative mRNA expression of occludin, claudin-5, zonula occludens ZO-1, and glucose transporter 1 (GLUT-1) in cerebral cavernous malformation (CCM) and control brain tissues. Data are shown as mean ± SEM in 2 separate experiments with 8 samples per group. Data were normalized against the endothelial cell marker gene *CD31*. The mRNA expression levels from controls (n = 8) are set as 100% (mean ± SEM). Differences in mRNA concentrations were determined by the Mann-Whitney-Wilcoxon test, with $p < 0.05$ being considered statistically significant. *** $p < 0.001$.

decreased, linear staining patterns of occludin, claudin-5, and ZO-1 could still be observed along EC-EC contacts in very few CCM foci. Therefore, further study is needed to determine whether a higher percentage of linear TJP arrangement at cell-cell borders correlates with the aggressive clinical behavior of CCMs, as suggested by others (20, 57). However, the mechanisms underlying expansion and rupture of CCMs remain uncertain (58).

Because TJP alterations correlate with a reduction of GLUT-1 in cerebral ECs, we also investigated GLUT-1 expression in CCMs. As expected, alterations in TJP distribution were accompanied by a marked downregulation of GLUT-1; vessel leakage was indicated by irregular fibronectin staining. In most CCM vessels, GLUT-1 immunoreactivity was completely absent, with a positive signal detected only in erythrocytes. Staining of red blood cells in extravascular CCM tissue suggests recent hemorrhage and serves as an internal positive control. The GLUT-1 is the only known endothelial BBB glucose transporter protein; therefore, its downregulation probably correlates with impaired glucose uptake and decreased cell metabolism (59).

The decrease in TJP and GLUT-1 protein immunoreactivity corresponded to modifications in gene expression. Therefore, differences in protein concentrations at TJs and EC plasma membranes are most likely caused by downregulation of mRNA expression. In addition, impaired TJP and GLUT-1 levels in CCM vessels may also correspond to protein redistribution within the tissue that could be influenced by alterations with further binding partners, such as impaired interactions with adherens junction components (AJs). The most important element of AJs consists of the VE-cadherin/β-catenin complex (60), and it is known that CCM1/Krit1 interacts with β-catenin; this in turn shows a cross reaction with TJs, probably in a Rap-1 GTPase–dependent manner (21, 61). Therefore, alterations in TJPs and GLUT-1 levels could influence or be caused by impairments in AJ protein components.

In conclusion, our data strongly support a fundamental role of TJ complexes and TJP in the pathophysiology of CCMs. We showed that CCMs have abnormal localizations of occludin, claudin-5, and ZO-1 at interendothelial contact sites, and that this is accompanied by a marked reduction of GLUT-1 expression. These alterations may affect vascular matrix stability and thus contribute to clinical progression in CCMs. Future studies will need to determine the interactions of TJPs with *CCM1*, *CCM2*, and *CCM3* gene products and other binding partners, such as AJ proteins. Furthermore, more information on the role of EC TJPs in the BBB in CCM will facilitate a better understanding of CCM behavior and may be beneficial in the development of an appropriate treatment.

ACKNOWLEDGMENTS

The authors thank the Center for Microscopy and Image Analysis, University of Zurich, for the use of the confocal microscope and technical assistance. The authors thank Mushfika Ahmad (Departments of Neurosurgery and Neurology, University Hospital, Zurich) for meticulous editorial revision and Dr Johannes Schmitt and Claudia Gottier (Division of Gastroenterology and Hepatology, University Hospital Zurich) for their assistance in RT-PCR analysis.

REFERENCES

1. Al-Shahi R, Bhattacharya JJ, Currie DG, et al. Prospective, population-based detection of intracranial vascular malformations in adults: The Scottish Intracranial Vascular Malformation Study (SIVMS). Stroke 2003;34:1163–69
2. Del Curling O Jr, Kelly DL Jr, Elster AD, et al. An analysis of the natural history of cavernous angiomas. J Neurosurg 1991;75:702–8
3. Rigamonti D, Hadley MN, Drayer BP, et al. Cerebral cavernous malformations. Incidence and familial occurrence. N Engl J Med 1988;319: 343–47
4. Leblanc GG, Golanov E, Awad IA, et al. Biology of vascular malformations of the brain. Stroke 2009;40:e694–e702
5. Rothbart D, Awad IA, Lee J, et al. Expression of angiogenic factors and structural proteins in central nervous system vascular malformations. Neurosurgery 1996;38:915–24; discussion 24–25
6. Kilic T, Pamir MN, Kullu S, et al. Expression of structural proteins and angiogenic factors in cerebrovascular anomalies. Neurosurgery 2000;46: 1179–91; discussion 91–92
7. Wustehube J, Bartol A, Liebler SS, et al. From the cover: Cerebral cavernous malformation protein CCM1 inhibits sprouting angiogenesis by activating DELTA-NOTCH signaling. Proc Natl Acad Sci U S A 2010; 107:12640–45
8. Mindea SA, Yang BP, Shenkar R, et al. Cerebral cavernous malformations: Clinical insights from genetic studies. Neurosurg Focus 2006:21;e1
9. Labauge P, Denier C, Bergametti F, et al. Genetics of cavernous angiomas. Lancet Neurol 2007;6:237–44
10. Gault J, Shenkar R, Recksiek P, et al. Biallelic somatic and germ line CCM1 truncating mutations in a cerebral cavernous malformation lesion. Stroke 2005;36:872–74
11. Akers AL, Johnson E, Steinberg GK, et al. Biallelic somatic and germ line mutations in cerebral cavernous malformations (CCMs): Evidence for a two-hit mechanism of CCM pathogenesis. Hum Mol Genet 2009; 18:919–30
12. Shenkar R, Venkatasubramanian PN, Wyrwicz AM, et al. Advanced magnetic resonance imaging of cerebral cavernous malformations: Part II. Imaging of lesions in murine models. Neurosurgery 2008;63:790–98; discussion 7–8
13. Plummer NW, Gallione CJ, Srinivasan S, et al. Loss of p53 sensitizes mice with a mutation in Ccm1 (KRIT1) to development of cerebral vascular malformations. Am J Pathol 2004;165:1509–18
14. Kleaveland B, Zheng X, Liu JJ, et al. Regulation of cardiovascular development and integrity by the heart of glass–cerebral cavernous malformation protein pathway. Nat Med 2009;15:169–76
15. Whitehead KJ, Chan AC, Navankasattusas S, et al. The cerebral cavernous malformation signaling pathway promotes vascular integrity via Rho GTPases. Nat Med 2009;15:177–84
16. Zhu Y, Wloch A, Wu Q, et al. Involvement of PTEN promoter methylation in cerebral cavernous malformations. Stroke 2009;40:820–26
17. Stockton RA, Shenkar R, Awad IA, et al. Cerebral cavernous malformations proteins inhibit Rho kinase to stabilize vascular integrity. J Exp Med 2010:207:881–96
18. Zhao Y, Tan YZ, Zhou LF, et al. Morphological observation and in vitro angiogenesis assay of endothelial cells isolated from human cerebral cavernous malformations. Stroke 2007;38:1313–19
19. Wong JH, Awad IA, Kim JH. Ultrastructural pathological features of cerebrovascular malformations: A preliminary report. Neurosurgery 2000; 46:1454–59
20. Clatterbuck RE, Eberhart CG, Crain BJ, et al. Ultrastructural and immunocytochemical evidence that an incompetent blood-brain barrier is related to the pathophysiology of cavernous malformations. J Neurol Neurosurg Psychiatry 2001;71:188–92
21. Glading A, Han J, Stockton RA, et al. KRIT-1/CCM1 is a Rap1 effector that regulates endothelial cell-cell junctions. J Cell Biol 2007;179: 247–54
22. Lischper M, Beuck S, Thanabalasundaram G, et al. Metalloproteinase mediated occludin cleavage in the cerebral microcapillary endothelium under pathological conditions. Brain Res 2010;1326:114–27

23. Cornford EM, Hyman S. Localization of brain endothelial luminal and abluminal transporters with immunogold electron microscopy. NeuroRx 2005;2:27–43
24. Rosenberg GA, Yang Y. Vasogenic edema due to tight junction disruption by matrix metalloproteinases in cerebral ischemia. Neurosurg Focus 2007;22:E4
25. Anderson JM, Van Itallie CM. Tight junctions and the molecular basis for regulation of paracellular permeability. Am J Physiol 1995;269:G467–G75
26. Tsukita S, Furuse M. Occludin and claudins in tight-junction strands: Leading or supporting players? Trends Cell Biol 1999;9:268–73
27. Furuse M. Molecular basis of the core structure of tight junctions. Cold Spring Harb Perspect Biol 2010;2:a002907
28. Fanning AS, Jameson BJ, Jesaitis LA, et al. The tight junction protein ZO-1 establishes a link between the transmembrane protein occludin and the actin cytoskeleton. J Biol Chem 1998;273:29745–53
29. Feldman GJ, Mullin JM, Ryan MP. Occludin: Structure, function and regulation. Adv Drug Deliv Rev 2005;57:883–917
30. McCarthy KM, Skare IB, Stankewich MC, et al. Occludin is a functional component of the tight junction. J Cell Sci 1996;109:2287–98
31. Dobrogowska DH, Vorbrodt AW. Quantitative immunocytochemical study of blood-brain barrier glucose transporter (GLUT-1) in four regions of mouse brain. J Histochem Cytochem 1999;47:1021–30
32. Gerhart DZ, LeVasseur RJ, Broderius MA, et al. Glucose transporter localization in brain using light and electron immunocytochemistry. J Neurosci Res 1989;22:464–72
33. Lippoldt A, Kniesel U, Liebner S, et al. Structural alterations of tight junctions are associated with loss of polarity in stroke-prone spontaneously hypertensive rat blood-brain barrier endothelial cells. Brain Res 2000;885:251–61
34. Birnbaum MJ, Haspel HC, Rosen OM. Cloning and characterization of a cDNA encoding the rat brain glucose-transporter protein. Proc Natl Acad Sci U S A 1986;83:5784–88
35. Fukumoto H, Seino S, Imura H, et al. Sequence, tissue distribution, and chromosomal localization of mRNA encoding a human glucose transporter-like protein. Proc Natl Acad Sci U S A 1988;85:5434–38
36. Pardridge WM, Boado RJ, Farrell CR. Brain-type glucose transporter (GLUT-1) is selectively localized to the blood-brain barrier. Studies with quantitative Western blotting and in situ hybridization. J Biol Chem 1990; 265:18035–40
37. Yadla S, Jabbour PM, Shenkar R, et al. Cerebral cavernous malformations as a disease of vascular permeability: From bench to bedside with caution. Neurosurg Focus 2010;29:E4
38. Ishihara H, Kubota H, Lindberg RL, et al. Endothelial cell barrier impairment induced by glioblastomas and transforming growth factor beta2 involves matrix metalloproteinases and tight junction proteins. J Neuropathol Exp Neurol 2008;67:435–48
39. Al-Shahi Salman R, Berg MJ, Morrison L, et al. Hemorrhage from cavernous malformations of the brain: Definition and reporting standards. Angioma Alliance Scientific Advisory Board. Stroke 2008;39:3222–30
40. Kivelev J, Niemela M, Kivisaari R, et al. Long-term outcome of patients with multiple cerebral cavernous malformations. Neurosurgery 2009;65: 450–55; discussion 5
41. van Swieten JC, Koudstaal PJ, Visser MC, et al. Interobserver agreement for the assessment of handicap in stroke patients. Stroke 1988;19:604–7
42. Di Iorio E, Barbaro V, Ferrari S, et al. Q-FIHC: Quantification of fluorescence immunohistochemistry to analyze p63 isoforms and cell cycle phases in human limbal stem cells. Microsc Res Tech 2006;69:983–91
43. Nagy Z, Peters H, Huttner I. Fracture faces of cell junctions in cerebral endothelium during normal and hyperosmotic conditions. Lab Invest 1984;50:313–22
44. Furuse M, Hirase T, Itoh M, et al. Occludin: A novel integral membrane protein localizing at tight junctions. J Cell Biol 1993;123:1777–88
45. Nitta T, Hata M, Gotoh S, et al. Size-selective loosening of the blood-brain barrier in claudin-5–deficient mice. J Cell Biol 2003;161: 653–60
46. Ohtsuki S, Sato S, Yamaguchi H, et al. Exogenous expression of claudin-5 induces barrier properties in cultured rat brain capillary endothelial cells. J Cell Physiol 2007:210;81–86
47. Harhaj NS, Antonetti DA. Regulation of tight junctions and loss of barrier function in pathophysiology. Int J Biochem Cell Biol 2004;36: 1206–37
48. Hawkins BT, Davis TP. The blood-brain barrier/neurovascular unit in health and disease. Pharmacol Rev 2005;57:173–85
49. Bolton SJ, Anthony DC, Perry VH. Loss of the tight junction proteins occludin and zonula occludens-1 from cerebral vascular endothelium during neutrophil-induced blood-brain barrier breakdown in vivo. Neuroscience 1998;86:1245–57
50. Citi S. The molecular organization of tight junctions. J Cell Biol 1993; 121:485–89
51. Vorbrodt AW, Dobrogowska DH, Tarnawski M. Immunogold study of interendothelial junction-associated and glucose transporter proteins during postnatal maturation of the mouse blood-brain barrier. J Neurocytol 2001;30:705–16
52. Forster C. Tight junctions and the modulation of barrier function in disease. Histochem Cell Biol 2008;130:55–70
53. Argaw AT, Gurfein BT, Zhang Y, et al. VEGF-mediated disruption of endothelial CLN-5 promotes blood-brain barrier breakdown. Proc Natl Acad Sci U S A 2009;106:1977–82
54. Kebir H, Kreymborg K, Ifergan I, et al. Human TH17 lymphocytes promote blood-brain barrier disruption and central nervous system inflammation. Nat Med 2007;13:1173–75
55. Sakakibara A, Furuse M, Saitou M, et al. Possible involvement of phosphorylation of occludin in tight junction formation. J Cell Biol 1997;137: 1393–401
56. Wachtel M, Bolliger MF, Ishihara H, et al. Down-regulation of occludin expression in astrocytes by tumor necrosis factor (TNF) is mediated via TNF type-1 receptor and nuclear factor-kappaB activation. J Neurochem 2001;78:155–62
57. Tu J, Stoodley MA, Morgan MK, et al. Ultrastructural characteristics of hemorrhagic, nonhemorrhagic, and recurrent cavernous malformations. J Neurosurg 2005;103:903–9
58. Fujimura M, Watanabe M, Shimizu H, et al. Expression of matrix metalloproteinases (MMPs) and tissue inhibitor of metalloproteinase (TIMP) in cerebral cavernous malformations: Immunohistochemical analysis of MMP-2, -9 and TIMP-2. Acta Neurochir (Wien) 2007;149: 179–83; discussion 83
59. Hou WK, Xian YX, Zhang L, et al. Influence of blood glucose on the expression of glucose transporter proteins 1 and 3 in the brain of diabetic rats. Chin Med J (Engl) 2007;120:1704–9
60. Dejana E, Corada M, Lampugnani MG. Endothelial cell-to-cell junctions. FASEB J 1995;9:910–18
61. Birukova AA, Zebda N, Fu P, et al. Association between adherens junctions and tight junctions via Rap1 promotes barrier protective effects of oxidized phospholipids. J Cell Physiol 2011;226:2052–62

